ACS APPLIED MATERIALS & INTERFACES

Research Article

www.acsami.org

Magnetic Nanocomposite Hydrogel Prepared by ZnO-initiated Photopolymerization for La (III) Adsorption

Xiangning Zheng, Dongbei Wu,* Teng Su, Song Bao, Chuanan Liao, and Qigang Wang*

Department of Chemistry, and Advanced Research Institute, Tongji University, Shanghai 200092, P.R. China

Supporting Information

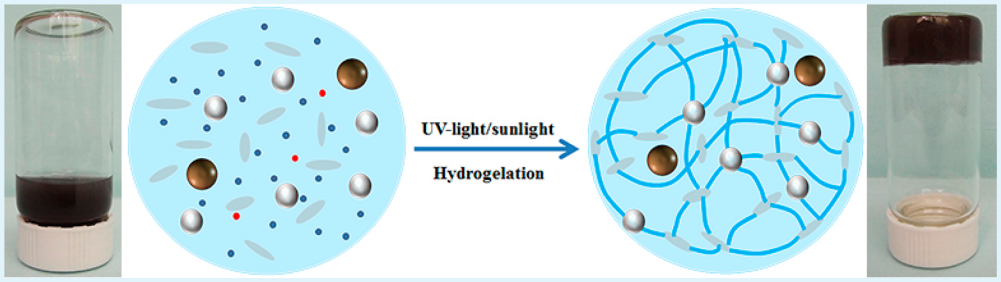

ABSTRACT: Here, we provide an effective method to fabricate magnetic ZnO clay nanocomposite hydrogel via the photopolymerization. The inorganic components endow the hydrogel with high mechanical strength, while the organic copolymers exhibit good adsorption capacity and separation selectivity to La (III) ions. An optimized hydrogel has the maximum compressive stress of 316.60 ± 15.83 kPa, which still exhibits 138.98 ± 7.32 kPa compressive strength after swelling. The maximum adsorption capacity of La ion is 58.8 mg/g. The adsorption matches the pseudo-second-order kinetics model. La (III) ions can be effectively separated from the mixtures of La/Ni, La/Co, La/Cu, and La/Nd in a broad pH range (2.0 to 8.0). After six adsorption−desorption cycles, the hydrogel can maintain its adsorption capacity. This work not only provides a new approach to the synthesis of tough hydrogels under irradiation, but also opens up enormous opportunities to make full use of magnetic nanocomposite hydrogels in environmental fields.

KEYWORDS: *nanocomposite hydrogel, ZnO, clay, magnetic separation, La (III) adsorption*

1. INTRODUCTION

Rare earth related materials are receiving considerable attentions and increasingly demanded in hi-tech industries because of their novel properties. Recently, they have been found wide applications in batteries, electronics, and chemical engineering.[1] Among them, lanthanum is practically used as metal, catalytic, and fluorescent materials.[2,3] The wide use of rare earth elements, whether free or complex, would finally lead to environmental problems in future. Therefore, an economical technique should be explored to recover the rare earth ions.[4,5]

The traditional approaches for the removing of lanthanides include ion-exchange, extraction, precipitation, reverse osmosis, and adsorption.[6−8] The adsorption is a promising technique because of the facile and economical operation. Such materials for the adsorption of lanthanide ions have biosorbents,[9−13]carbon materials,[14,15] silica materials,[16] other inorganic materials,[17−22] and polymer materials.[23−25] Hydrogels with three-dimensional hydrophilic networks have emerged as effective adsorbent because of its water-rich porous structure[26,27] and the functional polymer matrix with the amino, carboxyl, acylamino and sulfonic groups attached.[28−31]

However, most hydrogels suffer from a lack of mechanical strength, which usually makes them brittle and limits their further industrial applications. The typical tough hydrogels include the nanocomposite gels, the double-network gels, microsphere gels, and the ring-slide gels.[32−42] Among them, clay based nanocomposite hydrogel has received special attention because of its excellent mechanical strength.[43] Recently, our group developed a photopolymerized method for the preparation of tough clay-based nanocomposite hydrogels, where TiO_2 nanoparticle was employed as a photoinitiator to produce free radicals for polymerization.[44−46]

Herein, the magnetic nanoparticles were introduced into the tough hydrogel networks since it is well-known that magnetic adsorbent can be quickly and conveniently separated from the solution via an external magnetic field. It was revealed that the separation speed of adsorbent from adsorbate could be significantly enhanced with the help of magnetic field. ZnO nanoparticle, another inorganic semiconductor material, was used as a photoinitiator because of its suitable bandgap and photocatalytic performance similar to those of TiO_2 nanoparticle. Clay nanosheets were employed as cross-linkers and nanofillers to enhance mechanical strength of hydrogels. The selected monomers are N, N-dimethylacrylamide (DMAA) and 2-methylpropanesulfonic acid sodium (AMPSNa). A small amount of AMPSNa could improve the adsorption capacity

Received: August 5, 2014
Accepted: October 27, 2014
Published: October 27, 2014

 © 2014 American Chemical Society

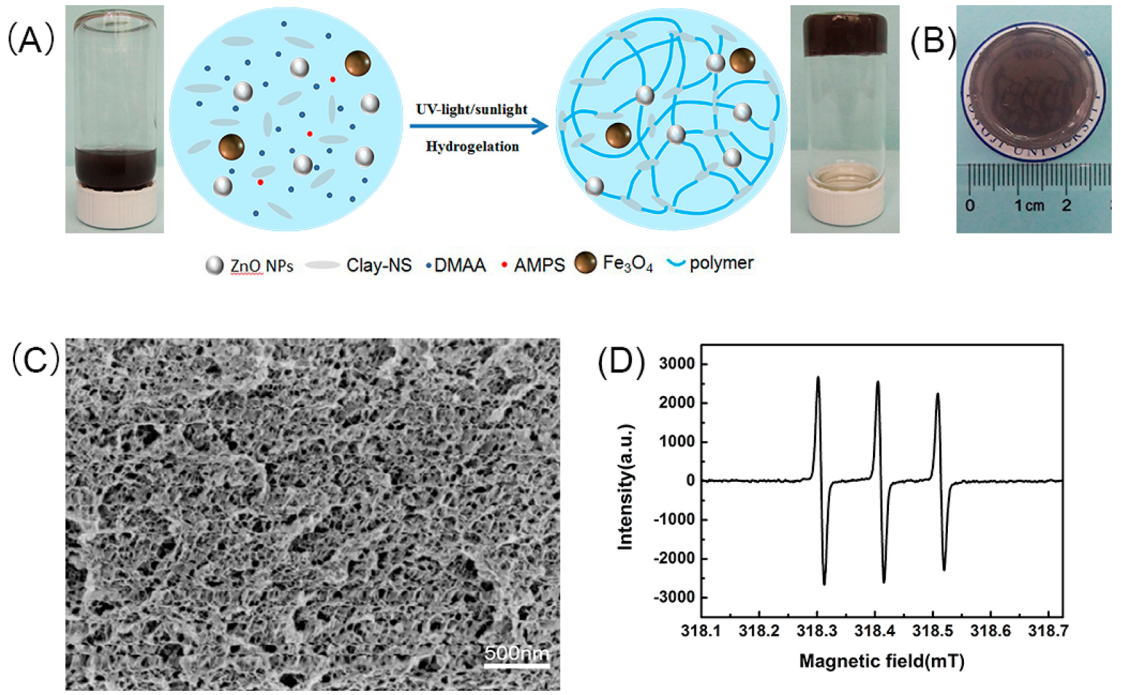

Figure 1. (A) Schematic preparation of magnetic nanocomposite hydrogel via ZnO-initiated polymerization. (B) Photograph of a self-standing hydrogel. (C) SEM image of a magnetic nanocomposite hydrogel after supercritical drying. (D) The EPR spectrum of the precursor comprising ZnO and DMAA under UV irradiation.

greatly. We anticipated exploring a universal method to prepare magnetic tough hydrogel for the application in the environmental field. Apart from the removal of metal ions, this water-rich material can also be employed for the removal of organic pollutant, particulate matter, cells, microbiological and viruses. It is expected that this work can not only provide a new facile approach to the synthesis of tough hydrogels under UV irradiation, but also open up enormous opportunities for environmental applications.

2. EXPERIMENTAL SECTION

2.1. Materials. DMAA (purity ≥99.0%) was purchased from TCI (Shanghai). AMPS (purity≥ 98%) was bought from Alfar Aesar. Clay nanosheet (Clay-NS with molecular formula: $Mg_{5.34}Li_{0.66}Si_8O_{20}(OH)_4$) was obtained from Rockwood Ltd. The dispersion of ZnO nanoparticles with about 10−30 nm size was got from Yicheng Ruijing (Beijing). Analytical grade reagents such as $LaCl_3$, $Co(NO_3)_2{\cdot}6H_2O$, $Ni(NO_3)_2{\cdot}6H_2O$, $CuSO_4{\cdot}5H_2O$, and $NdCl_3$ were obtained from Sinopharm (Shanghai). All the chemicals were used as received. Magnetic Fe_3O_4 nanoparticles with 200 ± 50 nm size were synthesized according to our earlier work.[16]

2.2. Preparation of Magnetic Nanocomposite Hydrogel. In our experiment, hydrogel was prepared from a homogeneous precursor aqueous solution composed of ZnO nanoparticles, Fe_3O_4 magnetic nanoparticles, Clay-NS, DMAA, and AMPSNa. The weakly basic environment (pH 9.0) is beneficial to the irradiation of ZnO nanoparticles and the production of OH radicals. It was confirmed that the OH radicals and holes were two initiating species for the formation of DMAA radicals and further propagating radicals.[44] Figure 1A shows that the magnetic nanocomposite hydrogel could be produced after 2 h UV light (middle-pressure mercury lamp, 100 $mW{\cdot}cm^{-2}$). As a typical example, 5.0% Clay-NS, 5.0% monomers (4.55% DMAA with 0.45% AMPSNa), 0.8% ZnO, and 0.06% Fe_3O_4 nanoparticles were employed to produce a magnetic ZnO clay nanocomposite hydrogel with considerable mechanical strength and magnetic properties. The total mass of precursor aqueous solution was 5.0 g. The as-obtained hydrogel samples were supercritically dried for SEM characterization and freeze-dried overnight for other experiments in view of the expensive operation cost of supercritical drying.

2.3. Characterizations. The morphology and microstructure of the supercritically dried hydrogels were characterized by a field emission SEM (Hitachi S 4800). A laser diffraction particle size analyzer (Eyetech-combo) was employed to measure the size and specific area of the freeze-dried hydrogel powder. A zeta potential instrument (zetasizer Nano Z) was used for determining the surface charge of hydrogel with various pH. The XRD patterns were obtained on a diffractometer (Philips APD-10) with Cu Kα radiation from 20° to 70°. Phase identification was confirmed by the JCPDS PDF database. The magnetization curve was measured by a vibrating sample magnetometer (Lakeshore 7400). FI-IR spectra was measured in a Fourier-transform infrared spectrometer (Nicolet Avatar 360) from 4000 to 400 cm^{-1}. A cylindrical gel sample with 25.0 ± 0.1 mm diameter and 13.2 ± 0.1 mm thickness was prepared before the mechanical analysis. A tensile-compressive tester (FR-108B) was employed to record the compressive stress−strain curves with 1.0 $mm{\cdot}min^{-1}$rate. The compressive strength and Young's modulus of hydrogels were calculated by 95% compression and the ratio from 5% to 15%, respectively. All the data were obtained from three independent measurements.

2.4. Swelling Studies. For the swelling studies, the hydrogel discs should be dried at 100 °C. The swelling ratio of hydrogels was investigated by gravimetric method. The dry hydrogel discs were swollen in excessive water for 30 h at room temperature. The wet gels were taken from water and dried by tissue paper to get the accurate weight. The saturated swelling ratio (S_R) was obtained by eq 1

$$S_R = \frac{W_S - W_d}{W_d} \quad (1)$$

where W_S and W_d denotes the saturated and dried weights, respectively. The data were averaged from five independent measurements.

2.5. Adsorption Experiments. The adsorptions were performed in a batch of models at room temperature. Typically, for pH effect on the adsorption, 30 mg hybrid hydrogel powders were immersed into 30 mL aqueous solution for 2 h. The concentration of metal ions

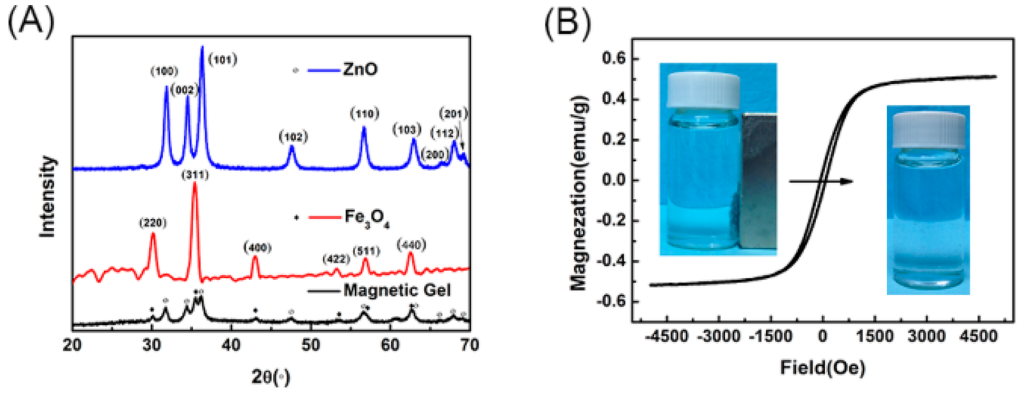

Figure 2. (A) XRD patterns of ZnO nanoparticles, magnetic Fe_3O_4 nanoparticles, and freeze-dried magnetic nanocomposite hydrogel. (B) Room temperature hysteresis loops of freeze-dried magnetic nanocomposite hydrogel powder. Left inset shows that the hydrogel powders dispersed in liquid can be magnetically collected by an external magnet. Right inset displays that the hybrid hydrogel powders can be redispersed into the solution readily.

including La^{3+}, Nd^{3+}, Cu^{2+}, Co^{2+}, and Ni^{2+}, was fixed at 0.3 mmol/L. The initial pH value ranged from 1.5 to 7.0. No buffer solution was used since the ionic strength would suppress the swelling of hydrogel. For La (III) adsorption isotherm experiment, 30 mg adsorbent was poured into a solution with the volume of 30 mL. The concentration of La (III) ion was from 0.03 to 1.6 mmol/L (4.0−220.0 mg/L) with pH 5.0. After 2 h adsorption, the hydrogel powders were directly separated from the solution by the magnet. The residue metal ion was measured by a UV−vis spectrophotometer. Arsenazo (III) was used to measure La^{3+} and Nd^{3+},[47,48] 4-(2-pyridylazo)resorcinol for Co^{2+} and Ni^{2+},[49,50] and sodium diethyldithiocarbamate for Cu^{2+},[51] respectively. The data were averaged from three independent measurements. The amount of metal ion within the adsorbent was calculated from eq 2:

$$q_e = \frac{(C_{ini} - C_e)V}{m} \quad (2)$$

where q_e is the adsorbed amount of La (III)(mg/g), C_{ini} and C_e are the starting and residue amount of La (III) (mg/L), respectively, V (L) is the solution volume, and m (g) is the weight of the hydrogel powder.

The uptake percentage (%), distribution ratio (D), and separation factor (S) were calculated by the following equations, eqs 3−5:

$$\%\text{uptake} = \frac{C_{ini} - C_e}{C_{ini}} \times 100 \quad (3)$$

$$D = q_e/(q_{ini} - q_e) \quad (4)$$

$$S = D_1/D_2 \quad (5)$$

For the interference experiment, the two-component system was composed of La^{3+} with K^+, Na^+, Ba^{2+}, Cd^{2+}, Co^{2+}, Mn^{2+}, Zn^{2+}, Ce^{3+}, respectively. The concentrations of La^{3+} ions was 3.0 mg/L, alkaline ions of 300 mg/L and the other metal ions of 30 mg/L. After the competitive adsorption, the residual La (III) ions in solution were analyzed via the ICP-OES. For the regeneration experiment, HCl aqueous solution (5.0 mL, 2.0 mol/L) was used as a desorption agent to regenerate the hybrid hydrogel after 2 h shaking. Then, the reused hydrogel powders were washed by sodium acetate buffer and distilled water repeatedly for three times. The data were averaged from three independent measurements.

3. RESULTS AND DISCUSSION

3.1. Synthesis, Mechanism, and Characterization. Figures 1B exhibits the appearance of a bulk hydrogel. The brown-black hydrogel is smooth and elastic and can be deformed into any shape. The water content within the hybrid hydrogel was estimated to be more than 89%. The SEM images in Figure 1C indicate that the supercritical dried hydrogel has porous structure with several tens nanometers size. Such loosely porous structure of the dried hydrogel is beneficial to the continuous application and the possible rapid adsorption kinetics.

The polymerization mechanism can be described as follows. At first, the ZnO nanoparticles produce photogenerated electrons and holes under UV irradiation. Such photogenerated holes with high oxidability can react with OH^- to produce OH radicals. The holes can attack the noncovalently adsorbed monomers to obtain the surface carbon radicals that directly initiate the polymerization at the nanoparticle surfaces. Both the active OH radicals and surface monomer radicals can initiate the polymerization around the ZnO nanoparticles. In order to confirm the polymerization mechanism, electron spin resonance (EPR) analysis was performed for the ZnO nanoparticles dispersion mixed with or without monomer. As expected, a set of peaks with a 1:2:2:1 ratio in the EPR spectrum revealed the existence of OH radical, similarly to the earlier work.[44] The signals of the propagating carbon radical with a 1:1:1 ratio confirmed the occurrence of polymerization in the presence of monomers (Figure 1D).

Figure 2 exhibits the XRD patterns (Figure 2A) and saturation magnetization curve (Figure 2B) of the magnetic nanocomposite hydrogel. The characteristic peaks of single Fe_3O_4 (2θ = 30.1, 37.1, 43.1, 53.4, 57.0, and 62.6) and the characteristic peaks of single ZnO (2θ = 31.5, 34.2, 36.0, 47.3, 56.4, 62.7, 66.2, 67.7, and 68.9) are both found in the XRD patterns of the hybrid hydrogel, which indicate the remained crystalline phases of Fe_3O_4 and ZnO nanoparticles. The magnetic property of the hybrid hydrogel was investigated for the feasibility of magnetic separation and regeneration of this adsorbent. The magnetic nanocomposite hydrogel has magnetic saturation value (M_s = 0.51 emu/g), coercivity (H_c = 72.55 Oe), and remanence (M_r = 0.05 emu/g), respectively (Figure 2B). The weak magnetic property for the magnetic nanocomposite hydrogel is mainly due to the low concentration of Fe_3O_4 (0.06 wt %). From a practical viewpoint, a material with a magnetic saturation value at least 30 emu/g (for μm-mm sized particle) is considered to be appropriate for magnetic separation in practice. However, for our hydrogel system, when the concentration of magnetic nanoparticle was more than 0.06%, the hydrogel could not be formed under irradiation because of the strong light absorption ability of dark Fe_3O_4. Moreover, excessive magnetic particles would cause a low

Table 1. Mechanical Properties of the Magnetic ZnO Nanocomposite Hydrogels with Different Compositions

sample	DMAA/AMPSNa (wt %)	clay (wt %)	ZnO (wt %)	Fe_3O_4 (wt %)	gelation	Young's modulus (kPa)	compressive stress (kPa)
1-1	5/0	5	0.2	0	P.G.[a]		
1-2	5/0	5	0.4	0	C.G.[b]	5.62 ± 0.28	242.05 ± 12.10
1-3	5/0	5	0.6	0	C.G.[b]	10.01 ± 0.50	274.24 ± 13.71
1-4	5/0	5	0.8	0	C.G.[b]	13.55 ± 0.68	319.51 ± 15.98
1-5	5/0	5	1.0	0	C.G.[b]	11.28 ± 0.56	285.43 ± 14.27
2-1	5/0	5	0.8	0.02	C.G.[b]	14.19 ± 0.71	285.29 ± 14.26
2-2	5/0	5	0.8	0.04	C.G.[b]	12.28 ± 0.61	296.83 ± 14.84
2-3	5/0	5	0.8	0.06	C.G.[b]	15.71 ± 0.79	299.52 ± 14.98
2-4	5/0	5	0.8	0.08	P.G.[a]		
3-1	4.55/0.45	2	0.8	0.06	C.G.[b]		
3-2	4.55/0.45	3	0.8	0.06	C.G.[b]	5.05 ± 0.25	144.31 ± 7.22
3-3	4.55/0.45	4	0.8	0.06	C.G.[b]	6.83 ± 0.34	247.85 ± 12.39
3-4	4.55/0.45	5	0.8	0.06	C.G.[b]	17.45 ± 0.87	316.60 ± 15.83
3-4	4.55/0.45	5	0.8	0.06	C.G.[b]	12.18 ± 0.56	198.45 ± 9.31[d]
3-4	4.55/0.45	5	0.8	0.06	C.G.[b]	15.20 ± 0.25	138.98 ± 7.32[e]
3-5	4.55/0.45	6	0.8	0.06	S.A.[c]		
4-1	4.44/0.56	5	0.8	0.06	P.G.[a]		
4-2	4.38/0.62	5	0.8	0.06	P.G.[a]		
4-3	2.50/2.50	5	0.8	0.06	P.G.[a]		

[a]P.G.: Partly gelation. [b]C.G.: Completely gelation. [c]S.A.: Clay self- aggregate. [d]Swollen hydrogel in 0.02% NaCl solution. [e]Swollen hydrogel in H_2SO_4 solution with pH 5.0

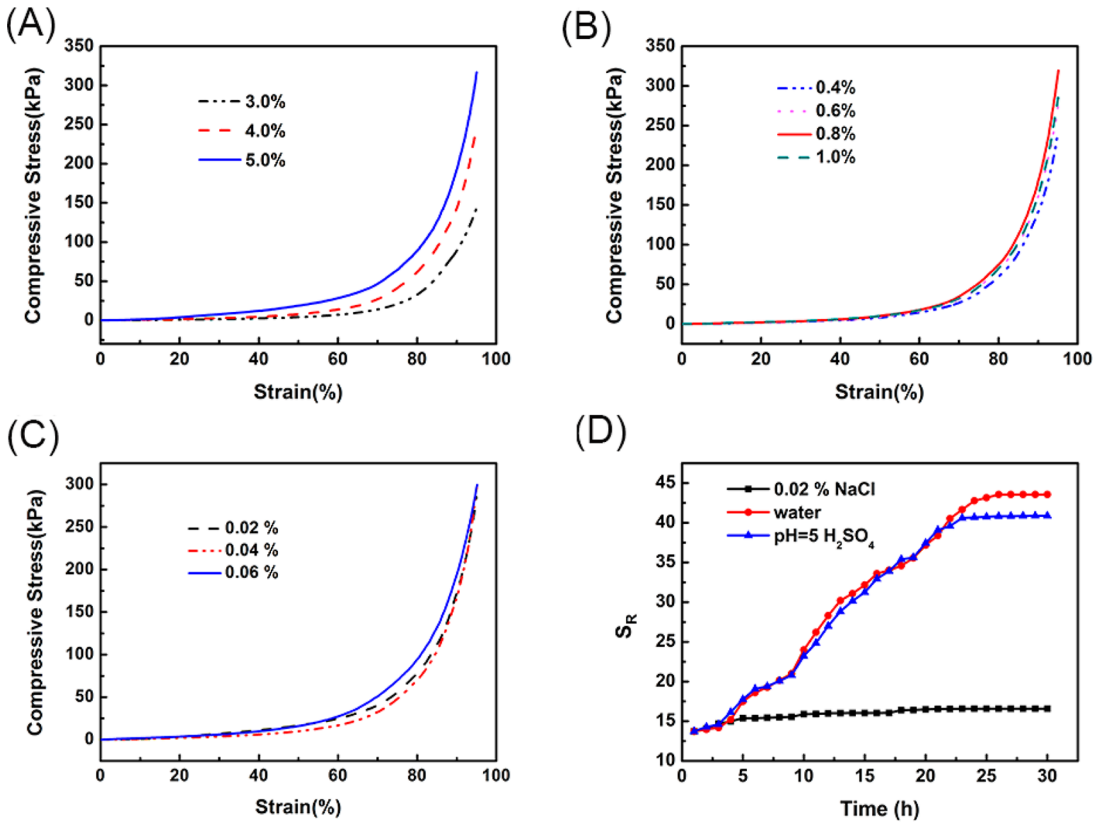

Figure 3. (A) Compressive test of the magnetic nanocomposite hydrogels with various clay amount. (B) Compressive test with various ZnO amount. (C) Compressive test with various Fe_3O_4 amount. (D) Swelling properties of the magnetic nanocomposite hydrogel.

adsorbed amount of La (III) ions by hydrogel powder.[10] Figure S1 (Supporting Information, SI) shows the average diameter and the specific area of our hydrogel particles were about 261 μm and 89.51 m^2/kg, respectively. The large size and high density make them separable by centrifugation or direct precipitation readily. The magnetic nanoparticles were employed to accelerate the gravity separation. As shown in Figure 2B left inset, the magnetic hydrogel powders could be collected quickly with a magnet. Furthermore, the magnetic nanoparticles were immobilized into the three-dimensional hydrogel network to effectively prevent the aggregation of magnetic particles. The final magnetic hydrogel powders could be redispersed in solution even though they had a certain

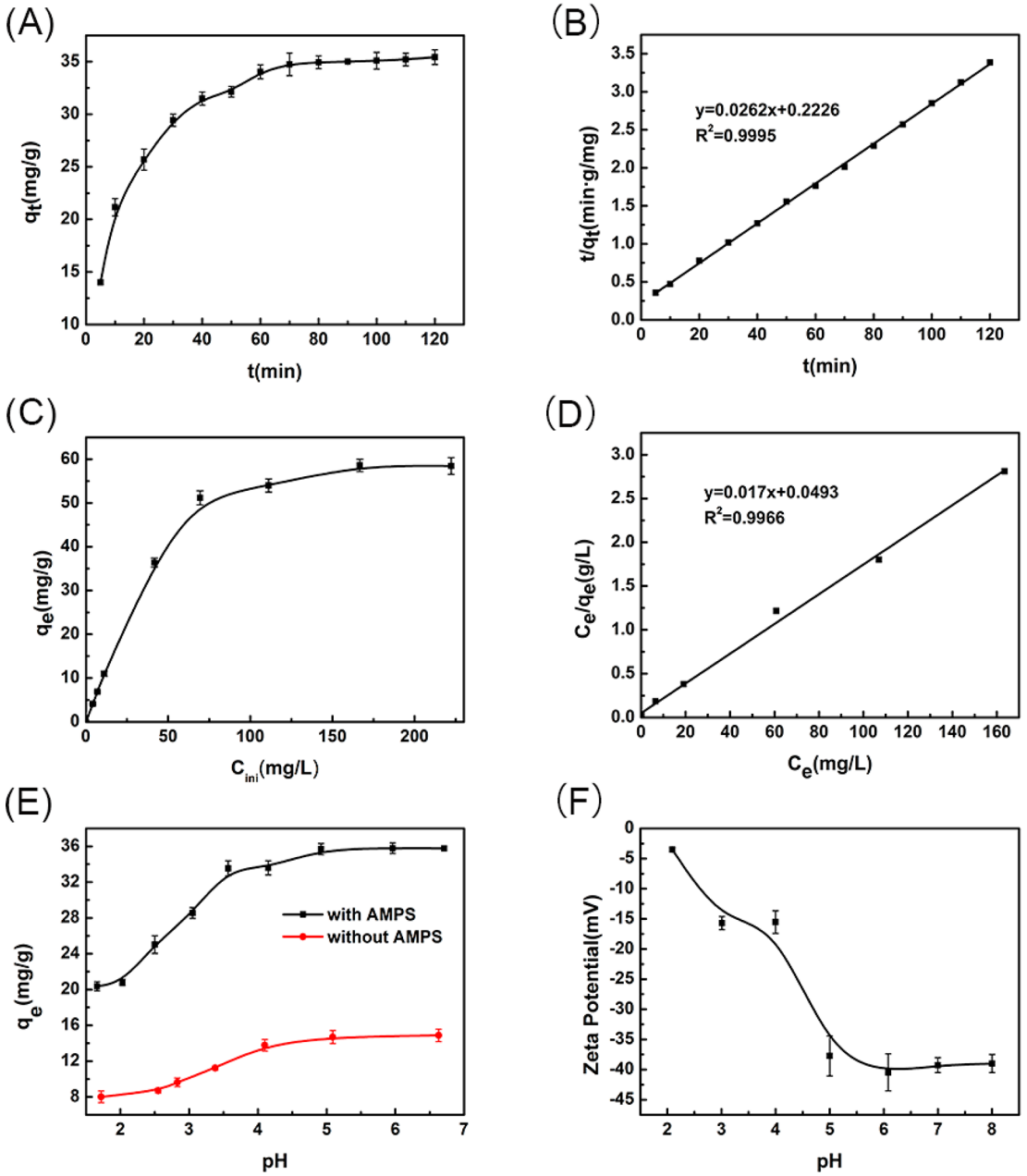

Figure 4. (A) Time-dependent capture and (B) adsorption kinetics via the pseudo-second-order model. The initial La (III) ion concentration is 42 mg/L(0.3 mmol/L) at an initial pH 5.0, and the sample dose is 30.0 mg per 30.0 mL. (C) The influence of La (III) ion concentration on the adsorption and (D) representative Langmuir isotherm, the initial ion concentration is 4.0−222.0 mg/L(0.03−1.60 mmol/L), pH of 5.0 and the sample dose is 30.0 mg per 30.0 mL. (E) pH effect on the adsorption with and without AMPSNa as a monomer, the initial ion concentration is 42.0 mg/L (0.3 mmol/L) and the sample dose is 30.0 mg per 30.0 mL. (F) Zeta potentials of hydrogel powders at various pH values.

remanent magnetization. The redispersion of the magnetic hydrogel powders is shown in the right inset of Figure 2B.

3.2. Mechanical Strength and Swelling Behavior. The magnetic nanocomposite hydrogel exhibits good mechanical performance. The compressive stress of hydrogel is highly dependent on the concentrations of all the components. The total concentration of organic monomer was selected to be 5.0% according to the earlier work.[31]Among the inorganic components, Clay-NS plays the most significant role in improving the mechanical strength. As shown in Table 1 and Figure 3A, both the Young's modulus and compressive stress enhance with an improvement of the concentration of Clay-NS from 2.0% to 5.0%. The value of compressive stress at strain of 95% increases from 144.31 ± 7.22 to 316.60 ± 15.83 kPa, while the value of Young's Modulus increases from 5.05 ± 0.25 to 17.45 ± 0.87 kPa correspondingly at the composition of 4.55% DMAA, 0.45% AMPSNa, 0.8% ZnO, and 0.06% Fe_3O_4. The Clay-NS could probably act as a cross-linking agent during hydrogelation so as to obviously enhance the mechanical strength. As the Clay-NS is negatively charged, the polymer chains formed from DMAA and AMPSNA could preferentially adsorb onto the surface and edge of Clay-NS before irradiation. Therefore, the optimal concentration of Clay-NS was 5.0%, which is also the maximum concentration of clay nanosheets that can be dispersed in water.

Similarly, the concentration of ZnO also has an influence on the compressive stress and Young's modulus of hybrid hydrogels, which is shown in Table 1 and Figure 3B. With the concentration of ZnO increasing from 0.4% to 1.0%, the value of compressive stress increased from 242.05 ± 12.10 to 319.51 ± 15.98 kPa, and then decreased to 285.43 ± 14.27 kPa. The values of Young's modulus increased from 5.62 ± 0.28 to 13.55 ± 0.68 kPa, then decreased to 11.28 ± 0.56 kPa, correspondingly. It is easy to understand that the mechanical strength increases with increasing concentration of ZnO as inorganic nanofiller. However, the excessive ZnO nanoparticles would lead to a heterogeneous hydrogel network. Consequently, the mechanical strength of hydrogel was reduced. The selected concentration of ZnO was 0.8%.

The concentration of Fe_3O_4 nanoparticle also has an influence on the mechanical strength, as shown in Table 1 and Figure 3C. As the concentration of Fe_3O_4 increased from 0.02% to 0.06%, the value of compressive stress was slightly enhanced from 285.29 ± 14.26 to 299.52 ± 14.98 kPa. The value of Young's modulus slowly increased from 14.19 ± 0.71 to 15.71 ± 0.79 kPa, correspondingly. When the concentration of Fe_3O_4 nanoparticle increased to 0.08%, the hydrogelation could not perform completely because Fe_3O_4 nanoparticle has a strong light absorption capacity. As the result, the photoelectric conversion efficiency of ZnO nanoparticles would be reduced greatly. Therefore, it was arbitrarily considered that the suitable concentration of Fe_3O_4 nanoparticle was 0.06%.

Figure 3D presents the swelling behavior of magnetic nanocomposite hydrogel in different media. It could be found that the swelling capacity in 0.02% NaCl solution was less than those in H_2SO_4 solution with pH 5.0, as well as in neutral water. The maximum equilibrium swelling ratio was 44 g/g in distilled water, 41 g/g in H_2SO_4 solution, and 17 g/g in 0.02% NaCl solution, respectively. The swollen hydrogel could reach approximately 42 times its dry weight and 1.7 times its original diameter (see Figure S2 in the Supporting Information). As listed in Table 1, the swollen hydrogel still has the maximum compressive strength of 139.98 ± 7.32 kPa (see Figure S3 in the Supporting Information). The excellent mechanical performance of hydrogel can resist the sewage erosion during wastewater treatment. It is obvious that the salt can reduce the swollen of hydrogel. Therefore, no additional electrolytes were used in the following adsorption experiments.

3.3. La (III) Adsorption and Hydrogels Recyclability. Figure 4A provides the time-dependent adsorbed curve of La (III) ions by the magnetic hydrogel powders. The adsorption proceed was quick and nearly reach equilibrium after 80 min. Therefore, a 120 min contact time was selected to reach adsorption equilibrium in the following experiments. Usually, the equilibrium time depends on the size, specific area, pore structure and surface charge of adsorbent. Short equilibrium time can be obtained by using the adsorbent with small size, large specific area, uniform pore structure and suitable surface charge. As far as hydrogel is concerned, it has a hydrophilic polymeric network, which will swell during adsorption. To describe the experimental results, different kinetic models were selected via linear or nonlinear regression. The pseudo-second-order equation can match the data (Figure 4B) with a high correlation coefficient (R^2 = 0.9995) and a close q_e value. The value of rate constant k_2 was calculated to be 3.08×10^{-3} g·mg^{-1}·min^{-1}. The differential eq 6 is written as follows:

$$\frac{t}{q_t} = \frac{1}{k_2 q_e^{\,2}} + \frac{t}{q_e} \tag{6}$$

In which q_t and k_2 denotes the adsorbed amount of La (III) ions onto the hydrogel at different times (min) and rate constant, respectively. By fitting the t/q_t against t plot, the values of slope of $1/q_e$ and intercept $1/k_2\, q_e^{\,2}$ can be calculated from the linear part of a straight line.

Figure 4C shows the concentration effect on the final adsorption. With increasing La (III) ion concentrations, the adsorption capacity increased progressively, and finally reached a saturation status. Various absorbed models were employed to match the La (III) ion adsorption within our hydrogel. For Langmuir isotherm, eq 7 is expressed as

$$\frac{C_e}{q_e} = \frac{C_e}{q_{max}} + \frac{1}{bq_{max}} \tag{7}$$

where q_{max} is the maximum adsorption capacity of metal ion. The parameter b is related to the affinity of the absorbent and absorbate. The value of q_{max} and b can be calculated from the fitted line of C_e/q_e versus C_e. According to the isotherm equation, the values of the maximum adsorption capacity and correlation coefficient were 58.8 mg/g and 0.9966 (Figure 4D), respectively. For the Freundlich isotherm, the correlation coefficient (R^2 = 0.7202, see Figure S4 in the Supporting Information) was lower than that of Langmuir isotherm. The Langmuir model indicates a monolayer absorbed manner of the La (III) ions on the hydrogels powder via the functional groups.

In our earlier work, magnetic alginate gels were applied for the remove of La (III) ions. The maximum 123.5 mg/g adsorbed amount was due to the stronger affinity of carboxyl groups in alginate to La (III) ions. However, the disadvantages of such alginate gel beads were weak mechanical strength, long equilibrium time, and easy breakage after three reuses. Furthermore, compared other adsorbents reported in the earlier work[16] with our hydrogel, we found that the biosorbents and carbon-based materials exhibited satisfactory adsorption capacity. Nevertheless, more equilibrium time is required with a lack of the information on the regeneration and reuse. Silica nanocomposite and polymer materials displayed a comparable adsorption capacity and equilibrium time to our hydrogel. For bentonite and other inorganic materials, whether natural or modified, they suffered from the shortcomings in both adsorption capacity and regeneration cycle. Besides, our hydrogel has the advantages of facile preparation, tough mechanical property and easy functionalization over other adsorbents.

To evaluate the role of AMPSNa on the La (III) adsorption into the magnetic ZnO nanocomposite hydrogel, we conducted experiments to study the pH effect on La (III) adsorption in the range from 1.5 to 7.0. Other experimental parameters including La (III) ion concentration, adsorbent dose, adsorbate volume, contacting time and temperature are the same for the hydrogel with and without AMPSNa. It was evident that the adsorption was significantly affected by the initial pH for the systems. As shown in Figure 4E, the maximum adsorption capacity was achieved at initial pH 5.0. Lanthanum salts are not so well-known. The La (III) ions can coordinate with hydroxide at 1:1, 1:2, 1:3 and 5:9 ratios. Different speciation carries different charges with different ionic radii, which makes the adsorption become complicated. Hence, a speciation graph and

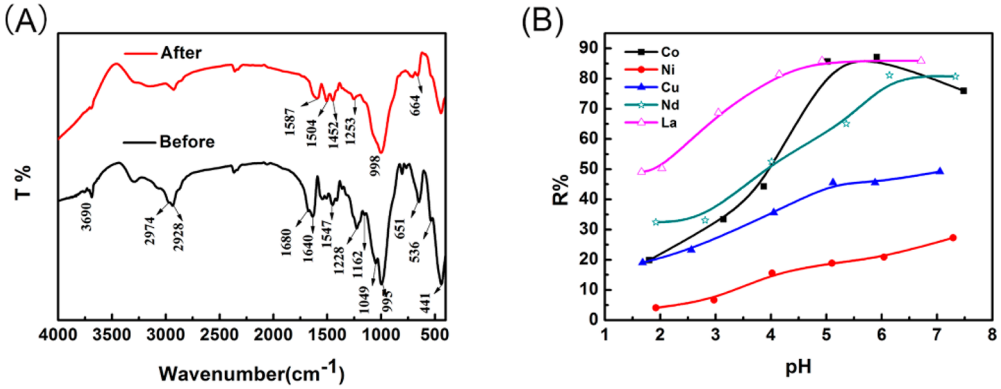

Figure 5. (A) FTIR of the pure hydrogel and the adsorbed one. (B) Separation selectivity of hydrogel with various metal ions.

consideration about the species found in specific conditions (concentration and pH) should be provided. The speciation diagram is reasonable for a broad concentration range of La (III) ions. According to the speciation diagram in the earlier work,[12] the predominant lanthanum species is $La_5(OH)_9^{6+}$ ions at equilibrium pH less than 4.0, La^{3+} ions at equilibrium pH from 6.0 to 8.0, $La(OH)^{2+}$at pH 12.0, and $La(OH)^{2+}$ at equilibrium pH from 12.0 to 14.0, respectively. It is considered that La^{3+} ions are the most suitable species for the adsorption investigation in view of its smaller diameter and more charges than other species. Moreover, to further explore the adsorption mechanism, zeta potential of hydrogel powder in the pH range from 2.0 to 8.0 were investigated as shown in Figure 4F. With increasing pH, the value of zeta potential decreased slowly from pH 2.0 to 5.0. Then, the value remained little change from pH 5.0 to 8.0. It is clear that the hydrogel powders could carry more negative charges at a higher pH value. The high pH was beneficial to the La (III) adsorption by the hydrogel powders. Therefore, the initial pH 5.0 was selected in the subsequent experiments.

For the hybrid hydrogel in a weak acidic solutions (pH value less than 4.0), whether with or without AMPSNa, exhibits low adsorption capacity of La (III), which might be attributed to the competitive adsorption between H^+ and $La_5(OH)_9^{6+}$. It is obvious that those adsorbates with small ionic radii and high concentration are adsorbed preferentially. With increasing pH values, La^{3+} ions became the main species, the concentration of H^+ decreased slowly and the surface charge of hybrid hydrogel become more negative. Consequently, the La (III) uptake increased gradually due to its high positive charge densities. The adsorption capacity of hydrogel with AMPSNa was higher than that of without AMPSNa. The sulfonic acid groups in AMPSNa should be the main reason, which has been proved by FTIR in Figure 5A. A typical absorption peak at 3690 cm^{-1} was attributed to the OH groups.[52] Other characteristic peaks at 995, 995 and 441 cm^{-1} suggested the existed bending of Al_2OH, Si−O−Al, and Si−O−Si, respectively.[53]Absorption peaks at 1640 and 1547 cm^{-1} were assigned to the C═O group and NH_2 groups in the DMAA and AMPSNa units, respectively.[54] The peaks at 1049 and 1162 cm^{-1} were the stretching vibrations of S═O bonds. The absorption peak at 651 cm^{-1} was attributed to the sulfonate groups in the polymer matrix.[55] After coordination with metal ions, the absorption peaks of C═O, NH_2, and sulfonate groups at 1640, 1547, and 651 cm^{-1} shifted to 1587, 1504 and 664 cm^{-1}, respectively. Furthermore, the absorption peaks at 1049 and 1162 cm^{-1} correlating to the S═O groups disappeared. On the basis of these results, it was confirmed that amide and sulfonic acid groups contributed to the La (III) adsorption.

To analyze the separation selectivity, the Cu^{2+}, Co^{2+}, Ni^{2+}, and Nd^{3+} were chosen for the adsorbed experiment with the same concentration at various pH. Figure 5B and Table 2 suggest the order of adsorption capacity is La^{3+}> Co^{2+} > Nd^{3+} > Cu^{2+} > Ni^{2+}. By comparing the values of separation coefficient, S, it can be known that La^{3+} ions could be effectively separated from the mixtures of La/Ni, La/Nd, and La/Cu systems over the entire pH range. The separation La (III) ions from the mixture of La/Co can be realized at the pH less than 5.0.

Table 2. Separation Coefficient Values of La/Co, La/Ni, La/Cu, and La/Nd at Different pH Values

pH	$S_{La/Co}$	$S_{La/Ni}$	$S_{La/Cu}$	$S_{La/Nd}$
2.0	4.07	23.56	3.48	2.10
3.0	4.39	30.77	5.57	4.45
4.0	5.50	23.72	5.10	3.99
5.0	1.02	26.23	2.86	3.28
6.0	0.90	23.07	3.03	1.42
7.0	1.92	16.16	2.55	1.45

The effect of foreign ions on adsorption was also investigated by the interfering testing of La (III) from the large amount of another ion onto the absorbent. The adsorption was performed in a two-component system (Table 3). No obvious change (removal of La^{3+} decreased from 99.2% to 98.4%) in the adsorption efficiency of La (III) could be found when 100-fold of K^+ or Na^+ was added. A slight reduction (removal of La^{3+} decreased from 99.2% to 92.8%) could be seen in the presence of 10-fold of Ba^{2+}, Cd^{2+}, Co^{2+} or Mn^{2+}. The ionic strength is the

Table 3. Effect of Interfering Ions on the Adsorption of La (III)

ions	compound	concentration ratio	removal of La^{3+} (%)	removal of interfering ions (%)
La^{3+}	$LaCl_3$		99.2	
K^+	KCl	100:1	98.4	2.1
Na^+	NaCl	100:1	98.5	2.2
Ba^{2+}	$BaCl_2$	10:1	95.0	0
Cd^{2+}	$CdCl_2$	10:1	94.9	2.0
Co^{2+}	$CoCl_2$	10:1	94.6	5.7
Mn^{2+}	$MnCl_2$	10:1	92.8	1.4
Zn^{2+}	$Zn(NO_3)_2$	10:1	89.7	0.4
Ce^{3+}	$Ce(NO_3)_3$	10:1	87.8	11.4

main reason for the small change in the adsorption efficiency. While the Zn^{2+} and Ce^{3+} have negative effect on the adsorbed amount. The removal of La (III) decreased from 99.2% to 87.8%, which might be due to the similar hydrated ionic radius of La^{3+} (1.15 Å) to Ce^{3+} ion (1.10 Å). Moreover, the anion ions had little effect on the adsorption of La (III) ions, indicating an excellent selectivity of hybrid hydrogels toward La (III) ion.

Reusing of hydrogel is important in the industrial applications due to the economic feasibility and resources conservations. To evaluate the reusability of the magnetic ZnO nanocomposite hydrogel, six adsorption−desorption cycles were measured for La (III) ion. The 5.0 mL of 2.0 M HCl was used as a stripping reagent. The elution ratio (%) was equal to the formula: Desorbed amount of La (III) ion/adsorbed amount of La (III) ion ×100, which are shown in Figure 6. In

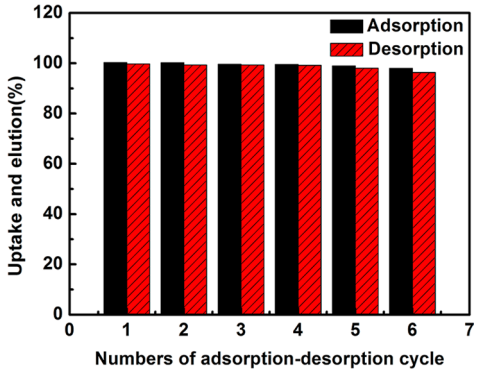

Figure 6. Reusability of the magnetic nanocomposite hydrogel for La (III) ions adsorption and desorption. For the adsorption process, the initial ion concentration is 35.0 mg/L, the pH is 5.0, and the adsorbent dose is 1.0 mg/mL. For the desorption process, the adsorbent dose is 6.0 mg/mL and that of HCl is 2.0 mol/L.

each adsorption−desorption cycle, almost 100% uptake and elution could be achieved at the initial concentration of La (III) of 35 mg/L and pH 5.0. Such measurement could be repeated at least six times. Except for a tiny loss of iron ion in the solution, no other change in mechanical and magnetic properties could be observed. These results indicate that our hydrogel holds great potential for practical applications.

4. CONCLUSIONS

In summary, a magnetic nanocomposite hydrogel was fabricated by a facile ZnO-initiated polymerization under UV irradiation. This approach is simple, effective and easy to operate in large scale. The as-prepared hydrogel exhibits high adsorption capacity (58.8 mg/g) and good selectivity toward La (III) ion. La (III) ions can be effectively separated from the mixtures of La/Co, La/Ni, La/Cu and La/Nd, systems in the pH range from 2.0 to 8.0. Because of its magnetic responsive behavior, the hydrogel can be readily collected from the adsorption media by an external magnet after adsorbing toxic metal ions. This magnetic nanocomposite hydrogel is also economically feasible as they can be reused for at least six cycles without obvious reduction in adsorption and desorption efficiencies. Moreover, the magnetic nanocomposite hydrogel would be particularly suitable for the photocatalytic degradation of organic pollutants, the treatment of toxic metal ions, and the recovery of valuables. It holds great promise as a potential multifunctional platform for environmental applications.

■ ASSOCIATED CONTENT

Supporting Information

Size distribution of the hydrogel powders in distilled water, the appearance of hydrogel in different swelling media, the compressive performance of hydrogel before and after swelling, and the fitting curve of Freundlich isotherm. This material is available free of charge via the Internet at http://pubs.acs.org.

■ AUTHOR INFORMATION

Corresponding Authors

*E-mail: wudongbei@tongji.edu.cn.
*E-mail: wangqg66@tongji.edu.cn.

Author Contributions

The manuscript was written through contributions of all authors. All authors have given approval to the final version of the manuscript.

Notes

The authors declare no competing financial interest.

■ ACKNOWLEDGMENTS

This work was financial supported by the National Natural Science Foundation of China (No. 21274111 and 51473123), the Program for New Century Excellent Talents in University of Ministry of Education of China (NECT-11-0386), and the Recruitment Program of Global Experts.

■ REFERENCES

(1) Vidal, K.; Ortega-San-Martin, L.; Larranaga, A.; Merino, R. I.; Orera, A.; Arriortua, M. I. Effects of Synthesis Conditions on the Structural, Stability and Ion Conducting Properties of $Li_{0.30}(La_{0.50}Ln_{0.50})_{0.567}TiO_3$ (Ln = La, Pr, Nd) Solid Electrolytes for Rechargeable Lithium Batteries. *Ceram. Int.* **2014**, *40*, 8761−8768.

(2) Yang, L. R.; Song, S.; Shao, C. Y.; Zhang, W.; Zhang, H. M.; Bu, Z. W.; Ren, T. G. Synthesis, Structure, and Luminescent Properties of Two-Dimensional Lanthanum(III) Porous Coordination Polymer Based on Pyridine-2,6-Dicarboxylic Acid. *Synth. Met.* **2011**, *161*, 925−930.

(3) Rabl, S.; Haas, A.; Santi, D.; Flego, C.; Ferrari, M.; Calemma, V.; Weitkamp, J. Ring Opening of Cis-Decalin on Bifunctional Ir/- and Pt/La-X Zeolite Catalysts. *Appl. Catal., A* **2011**, *400*, 131−141.

(4) Li, J. X.; Hong, M.; Yin, X. Q.; Liu, J. L. Effects of the Accumulation of the Rare Earth Elements on Soil Macrofauna Community. *J. Rare Earths* **2010**, *28*, 957−964.

(5) Moriwaki, H.; Koide, R.; Yoshikawa, R.; Warabino, Y.; Yamamoto, H. Adsorption of Rare Earth Ions onto the Cell Walls of Wild-Type and Lipoteichoic Acid-Defective Strains of *Bacillus subtilis*. *Appl. Microbiol. Biotechnol.* **2013**, *97*, 3721−3728.

(6) Murthy, Z. V. P.; Choudhary, A. Separation and Estimation of Nanofiltration Membrane Transport Parameters for Cerium and Neodymium. *Rare Met.* **2012**, *31*, 500−506.

(7) Nejad, S. J.; Abolghasemi, H.; Moosavian, M. A.; Maragheh, M. G. Fractional Factorial Design for the Optimization of Supercritical Carbon Dioxide Extraction of La^{3+}, Ce^{3+} and Sm^{3+} Ions from a Solid Matrix Using Bis(2,4,4-Trimethylpentyl)Dithiophosphinic Acid Plus Tributylphosphate. *Chem. Eng. Res. Des.* **2011**, *89*, 827−835.

(8) Kala, R.; Rao, T. P. Ion Imprinted Polymer Particles for Separation of Yttrium from Selected Lanthanides. *J. Sep. Sci.* **2006**, *29*, 1281−1287.

(9) Palmieri, M. C.; Volesky, B.; Garcia, O. Biosotption of Lanthanum Using Sargassum Fluitans in Batch System. *Hydrometallurgy* **2002**, *67*, 31−36.

(10) Wu, D. B.; Zhao, J.; Zhang, L.; Wu, Q. S.; Yang, Y. H. Lanthanum Adsorption Using Iron Oxide Loaded Calcium Alginate Beads. *Hydrometallurgy* **2010**, *101*, 76−83.

(11) Diniz, V.; Volesky, B. Biosorption of La, Eu and Yb Using Sargassum Biomass. *Water Res.* **2005**, *39*, 239−247.
(12) Wu, D. B.; Zhang, L.; Wang, L.; Zhu, B. H.; Fan, L. Y. Adsorption of Lanthanum by Magnetic Alginate−Chitosan Gel Beads. *J. Chem. Technol. Biotechnol.* **2011**, *86*, 345−352.
(13) Zhang, L.; Wu, D. B.; Zhu, B. H.; Yang, Y. H.; Wang, L. Adsorption and Selective Separation of Neodymium with Magne Alginate Microcapsules Containing the Extractant 2-Ethylhexyl Phosphonic Acid Mono-2-ethylhexyl Ester. *J. Chem. Eng. Data* **2011**, *56*, 2280−2289.
(14) Awwad, N. S.; Gad, H. M. H.; Ahmad, M. I.; Aly, H. F. Sorption of Lanthanum and Erbium from Aqueous Solution by Activated Carbon Prepared from Rice Husk. *Colloids Surf., B* **2010**, *81*, 593−599.
(15) Koochaki-Mohammadpour, S. M. A.; Torab-Mostaedi, M.; Talebizadeh-Rafsanjani, A.; Naderi-Behdani, F. Adsorption Isotherm, Kinetic, Thermodynamic, and Desorption Studies of Lanthanum and Dysprosium on Oxidized Multiwalled Carbon Nanotubes. *J. Dispersion Sci. Technol.* **2014**, *35*, 244−254.
(16) Wu, D. B.; Sun, Y. H.; Wang, Q. G. Adsorption of Lanthanum (III) from Aqueous Solution Using 2-Ethylhexyl Phosphonic Acid Mono-2-Ethylhexyl Ester-Grafted Magnetic Silica Nanocomposites. *J. Hazard. Mater.* **2013**, *260*, 409−419.
(17) Chegrouche, S.; Mellah, A.; Telmoune, S. Removal of Lanthanum from Aqueous Solutions by Natural Bentonite. *Water Res.* **1997**, *31*, 1733−1737.
(18) Chen, Y. G.; Zhu, C. M.; Sun, Y. H.; Duan, H. Y.; Ye, W. M.; Wu, D. B. Adsorption of La(III) onto GMZ Bentonite: Effect of Contact Time, Bentonite Content, pH Value and Ionic Strength. *J. Radioanal. Nucl. Chem.* **2012**, *292*, 1339−1347.
(19) Wu, D. B.; Zhu, C. M.; Chen, Y. G.; Zhu, B. H.; Yang, Y. H.; Wang, Q. G.; Ye, W. M. Preparation, Characterization and Adsorptive Study of Rare Earth Ions Using Magnetic GMZ Bentonite. *Appl. Clay Sci.* **2012**, *62*−*63*, 87−93.
(20) Chen, Y. G.; Zhu, B. H.; Wu, D. B.; Wang, Q. G.; Yang, Y. H.; Ye, W. M.; Guo, J. F. Eu(III) Adsorption Using Di(2-thylhexly) Phosphoric Acid-Immobilized Magnetic GMZ Bentonite. *Biochem. Eng. J.* **2012**, *181*, 387−396.
(21) Granados-Correa, F.; Vilchis-Granados, J.; Jimenez-Reyes, M.; Quiroz-Granados, L. A. Adsorption Behaviour of La(III) and Eu(III) Ions from Aqueous Solutions by Hydroxyapatite: Kinetic, Isotherm, and Thermodynamic Studies. *J. Chem.* **2013**, *2013*, 1−9.
(22) Li, S. Q.; Hu, B.; Jiang, Z. C.; Liang, P.; Li, X.; Xia, L. B. Selective Separation of La^{3+} and Lanthanum Organic Complexes with Nanometer-Sized Titanium Dioxide and Their Detection by Using Fluorination-Assisted Electrothermal Vaporization ICP-AES with in-Situ Matrix Removal. *Environ. Sci. Technol.* **2004**, *38*, 2248−2251.
(23) El-Sofany, E. A. Removal of Lanthanum and Gadolinium from Nitrate Medium Using Aliquat-336 Impregnated onto Amberlite XAD-4. *J. Hazard. Mater.* **2008**, *153*, 948−954.
(24) Maheswari, M. A.; Subramanian, M. S. Extraction Chromatographic Method for the Separation of Actinides and Lanthanides Using EDHBA Grafted AXAD-16 Polymer. *Talanta* **2005**, *65*, 735−742.
(25) Hong, G. S.; Shen, L. D.; Wang, M.; Yang, Y.; Wang, X. F.; Zhu, M. F.; Hsiao, B. S. Nanofibrous Polydopamine Complex Membranes for Adsorption of Lanthanum (III) Ions. *Chem. Eng. J.* **2014**, *244*, 307−316.
(26) Liu, X. H.; Wu, D. B.; Wang, H. L.; Wang, Q. G. Self-Recovering Tough Gel Electrolyte with Adjustable Supercapacitor Performance. *Adv. Mater.* **2014**, *26*, 4370−4375.
(27) Hua, R.; Li, Z. K. Sulfhydryl Functionalized Hydrogel with Magnetism: Synthesis, Characterization, and Adsorption Behavior Study for Heavy Metal Removal. *Chem. Eng. J.* **2014**, *249*, 189−200.
(28) Ramirez, E.; Burillo, S. G.; Barrera-Diaz, C.; Roa, G.; Bilyeu, B. Use of pH-Sensitive Polymer Hydrogels in Lead Removal from Aqueous Solution. *J. Hazard. Mater.* **2011**, *192*, 432−439.
(29) Chen, J. P.; Hong, L. A.; Wu, S. N.; Wang, L. Elucidation of Interactions between Metal Ions and Ca Alginate-Based Ion-Exchange Resin by Spectroscopic Analysis and Modeling Simulation. *Langmuir* **2002**, *18*, 9413−9421.
(30) Jin, L.; Bai, R. B. Mechanisms of Lead Adsorption on Chitosan/PVA Hydrogel Beads. *Langmuir* **2002**, *18*, 9765−9770.
(31) Bao, S.; Wu, D. B.; Wang, Q. G.; Su, T. Functional Elastic Hydrogel as Recyclable Membrane for the Adsorption and Degradation of Methylene Blue. *PLoS One* **2014**, *9*, No. e88802.
(32) Wang, J. Y.; Wang, Z. H.; Gao, J.; Wang, L.; Yang, Z. Y.; Kong, D. L.; Yang, Z. M. Incorporation of Supramolecular Hydrogels into Agarose Hydrogels—a Potential Drug Delivery Carrier. *J. Mater. Chem.* **2009**, *19*, 7892−7896.
(33) Wang, H. M.; Yang, Z. M. Short-Peptide-Based Molecular Hydrogels: Novel Gelation Strategies and Applications for Tissue Engineering and Drug Delivery. *Nanoscale* **2012**, *4*, 5259−5267.
(34) Su, T.; Zhang, D.; Tang, Z.; Wu, Q.; Wang, Q. G. HRP-Mediated Polymerization Forms Tough Nanocomposite Hydrogels with High Biocatalytic Performance. *Chem. Commun.* **2013**, *49*, 8033−8035.
(35) Wang, Q. G.; Mynar, J. L.; Yoshida, M.; Lee, E.; Lee, M.; et al. High-Water Content Mouldable Hydrogels by Mixing Clay and a Dendritic Molecular Binder. *Nature* **2010**, *463*, 339−343.
(36) Cong, H. P.; Ren, X. C.; Wang, P.; Yu, S. H. Macroscopic Multifunctional Graphene-Based Hydrogels and Aerogels by a Metal Ion Induced Self-Assembly Process. *ACS Nano* **2012**, *6*, 2693−2703.
(37) Haraguchi, K.; Murata, K.; Takehisa, T. Stimuli-Responsive Nanocomposite Gels and Soft Nanocomposites Consisting of Inorganic Clays and Copolymers with Different Chemical Affinities. *Macromolecules* **2012**, *45*, 385−391.
(38) Gao, G. R.; Du, G. L.; Cheng, Y. J.; Fu, J. Tough Nanocomposite Double Network Hydrogels Reinforced with Clay Nanorods through Covalent Bonding and Reversible Chain Adsorption. *J. Mater. Chem. B* **2014**, *2*, 1539−1548.
(39) Sun, J. Y.; Zhao, X.; Illeperuma, W. R. K.; Chaudhuri, O.; Oh, K. H.; et al. Highly Stretchable and Tough Hydrogels. *Nature* **2012**, *489*, 133−137.
(40) Chen, Q.; Zhu, L.; Huang, L. N.; Chen, H.; Xu, K.; Tan, Y.; Wang, P. X.; Zheng, J. Fracture of the Physically Cross-Linked First Network in Hybrid Double Network Hydrogels. *Macromolecules* **2014**, *47*, 2140−2148.
(41) Zhao, J.; Jiao, K. X.; Yang, J.; He, C. C.; Wang, H. L. Mechanically Strong and Thermosensitive Macromolecular Microsphere Composite Poly(N-Isopropylacrylamide) Hydrogels. *Polymer* **2013**, *54*, 1596−1602.
(42) Takehara, H.; Nagaoka, A.; Noguchi, J.; Akagi, T.; Sakai, T.; Chung, U.; Kasai, H.; Ichiki, T. Implementation of Tetra-Poly-(Ethylene Glycol) Hydrogel with High Mechanical Strength into Microfluidic Device Technology. *Biomicrofluidics* **2013**, *7*, 054109.
(43) Haraguchi, K. Nanocomposite Hydrogels: A Unique Organic-Inorganic Network Structure with Extraordinary Mechanical, Optical, and Swelling/Deswelling Properties. *Adv. Mater.* **2002**, *16*, 1120−1123.
(44) Zhang, D.; Yang, J. H.; Bao, S.; Wu, Q. S.; Wang, Q. G. Semiconductor Nanoparticle-Based Hydrogels Prepared via Self-Initiated Polymerization under Sunlight, Even Visible Light. *Sci. Rep.* **2013**, *3*, 1399.
(45) Liao, C. A.; Wu, Q.; Su, T.; Zhang, D.; Wu, Q. S.; Wang, Q. G. Nanocomposite Gels via in Situ Photoinitiation and Disassembly of TiO_2-Clay Composites with Polymers Applied as UV Protective Films. *ACS Appl. Mater. Interfaces* **2014**, *6*, 1356−1360.
(46) Liu, X. H.; Wen, Z. B.; Wu, D. B.; Wang, H. L.; Yang, J. H.; Wang, Q. G. Tough BMIMCl-Based Ionogels Exhibiting Excellent and Adjustable Performance in High-Temperature Supercapacitors. *J. Mater. Chem. A* **2014**, *2*, 11569−11573.
(47) Zuo, Y.; Chen, J.; Li, D. Q. Reversed Micellar Solubilization Extraction and Separation of Thorium(IV) from Rare Earth(III) by Primary Amine N1923 in Ionic Liquid. *Sep. Purif. Technol.* **2008**, *63*, 684−690.
(48) Liu, Y. H.; Chen, J.; Li, D. Q. Application and Perspective of Ionic Liquids on Rare Earths Green Separation. *Sep. Sci. Technol.* **2012**, *47*, 223−232.

(49) Ciftci, H. Solid Phase Extraction Method for the Determination of Cobalt in Water Samples on Duolite XAD-761 Resin Using 4-(2-Pyridylazo) Resorcinol by FAAS. *Curr. Anal. Chem.* **2010**, *6*, 154−160.
(50) Hol, A.; Divrikli, U.; Elci, L. Determination of Cobalt, Nickel and Iron at Trace Level in Natural Water Samples by in-Column Chelation-Reversed Phase High-Performance Liquid Chromatography. *Environ. Monit. Assess.* **2012**, *184*, 3469−3479.
(51) Munoz, C.; Toral, M. I.; Ahumada, I.; Richter, P. Rotating Disk Sorptive Extraction of Cu-Bisdiethyldithiocarbamate Complex from Water and Its Application to Solid Phase Spectrophotometric Quantification. *Anal. Sci.* **2014**, *30*, 613−617.
(52) Hatch, C. D.; Wiese, J. S.; Crane, C. C.; Harris, K. J.; Kloss, H. G.; Baltrasaitis, J. Water Adsorption on Clay Minerals as a Function of Relative Humidity: Application of BET and Freundlich Adsorption Models. *Langmuir* **2012**, *28*, 1790−1803.
(53) Zhu, B. H.; Wu, D. B.; Yang, Y. H.; Chen, Y. G.; Li, W. J.; Guo, J. F.; Wang, Q. G. Selective Removal of La(III) Ions Using Super-Paramagnetic Nanosorbent Coated by Saponified Sec-Octylphenoxy Acetic Acid. *J. Chem. Eng. Data* **2012**, *57*, 553−560.
(54) Kasgoz, H.; Durmus, A.; Kasgoz, A. Enhanced Swelling and Adsorption Properties of AAm-AMPSNa/Clay Hydrogel Nanocomposites for Heavy Metal Ion Removal. *Polym. Adv. Technol.* **2008**, *19*, 213−220.
(55) Layek, R. K.; Samanta, S.; Nandi, A. K. Graphene Sulphonic Acid/Chitosan Nano Biocomposites with Tunable Mechanical and Conductivity Properties. *Polymer* **2012**, *53*, 2265−2273.